TU Delft

Delft University of Technology

Artifact Interpretation of Spectral Response Measurements on Two-Terminal Multijunction Solar Cells

Si, Fai Tong; Isabella, Olindo; Zeman, Miro

DOI
10.1002/aenm.201601930

Publication date
2016

Document Version
Final published version

Published in
Advanced Energy Materials

Citation (APA)
Si, F. T., Isabella, O., & Zeman, M. (2016). Artifact Interpretation of Spectral Response Measurements on Two-Terminal Multijunction Solar Cells. *Advanced Energy Materials*, *7*(6), 1-14. Article 1601930. https://doi.org/10.1002/aenm.201601930

Important note
To cite this publication, please use the final published version (if applicable).
Please check the document version above.

Copyright
Other than for strictly personal use, it is not permitted to download, forward or distribute the text or part of it, without the consent of the author(s) and/or copyright holder(s), unless the work is under an open content license such as Creative Commons.

Takedown policy
Please contact us and provide details if you believe this document breaches copyrights.
We will remove access to the work immediately and investigate your claim.

This work is downloaded from Delft University of Technology.
For technical reasons the number of authors shown on this cover page is limited to a maximum of 10.

Artifact Interpretation of Spectral Response Measurements on Two-Terminal Multijunction Solar Cells

Fai Tong Si, Olindo Isabella, and Miro Zeman*

Multijunction solar cells promise higher power-conversion efficiency than the single-junction. With respect to two-terminal devices, an accurate measurement of the spectral response requires a delicate adjustment of the light- and voltage-biasing; otherwise it can result in artifacts in the data and thus misinterpretation of the cell properties. In this paper, the formation of measurement artifacts is analyzed by modeling the measurement process, that is, how the current–voltage characteristics of the component subcells evolve with the photoresponse to the incident spectrum. This enables the examination on the operation conditions of the subcells, offering additional information for the study of artifacts. In particular, the influence of shunt resistance, bias-light intensity, and bias voltage on the measurement is examined. Having observed the dynamics and vulnerability of the measurement, the proper ways to configure and interpret a measurement are discussed in depth. As a practical example, simulations of the measurements on a quadruple-junction thin-film silicon solar cell demonstrate that the modeling can be used to interpret eventual irregularities in the measured spectral response. The application of such tool is especially meaningful taking account of the diverse and rapid development of novel hybrid multijunction solar cells, in which the role of reliable characterizations is essential.

1. Introduction

Multijunction solar cells can reach higher power conversion efficiency than their single-junction counterparts by means of the better utilization of the photon energy in the solar spectrum.[1] They hold the highest record efficiencies across different branches of solar-cell technologies.[2–4] Typically, multijunction solar cells are made in a two-terminal structure because of the simple workflow of device fabrication as well as the straightforward design of electrical terminals. The component subcells are electrically connected in series such that the device has only two terminals to interact with the external circuit. As a consequence, the individual response of the subcells is not directly accessible, leading to restrictions on the device characterization.

The measurement of the spectral response or external quantum efficiency (EQE) requires specialized strategies when applied to two-terminal multijunction solar cells. Back in 1980s, certain procedures were proposed to measure the EQE of multijunction cells.[5] The basic idea is to measure the EQE of each subcell separately, i.e., only one subcell is examined at a time. Continuous light sources, which are referred to as the bias light, are used to generate photocarriers in the subcells. Having manipulated the bias spectrum, the targeted subcell provides the least potential photocurrent. Owing to the nature of series connection, this subcell limits the current of the multijunction cell. On top of the bias light, a periodically chopped monochromatic light source is used to excite additional photocarriers in the subcells. The resulting periodic perturbation in the external circuit, detected by a lock-in amplifier, represents the response of the current-limiting subcell to the incident monochromatic light. As a result, the EQEs of different subcells can be examined individually by adjusting the bias illumination. To improve the measurement, voltage biasing may be used in addition to light biasing. Conventionally, a bias voltage is applied such that the targeted subcell can operate like it is in its short-circuit condition.

Such measurement is susceptible to artifacts because of its indirect and dynamic essence of signal generation as well as the strong correlation between the subcells. Several possible measurement artifacts have been observed and discussed in literature. Based on the observations on GaInP/Ga(In)As/Ge triple-junction cells, Meusel et al. systematically studied the artifacts and associated them with the low shunt resistance or low reverse breakdown voltage of the subcell to be measured.[6] They also ascribed the artifact formation to the correlation between the operation points of the subcells. The measured signal including the artifacts can be affected by the bias condition. These effects have been discussed with the emphasis on either bias light[7–10] or bias voltage,[6,9,11–13] resulting in suggestions for mitigating certain measurement artifacts. Accordingly, to promote reliable measurements, comprehensive measurement procedures have been proposed in literature[6,14] and in a standard published by ASTM International.[15]

Although the mentioned literature can serve as useful guidelines for adjusting the measurement configuration, it does not

F. T. Si, Dr. O. Isabella, Prof. M. Zeman
Photovoltaic Materials and Devices Laboratory
Delft University of Technology
Mekelweg 4, Delft 2628 CD, The Netherlands
E-mail: f.t.si@tudelft.nl

This is an open access article under the terms of the Creative Commons Attribution-NonCommercial-NoDerivatives License, which permits use and distribution in any medium, provided the original work is properly cited, the use is non-commercial and no modifications or adaptations are made.

DOI: 10.1002/aenm.201601930

 © 2016 The Authors. Published by WILEY-VCH Verlag GmbH & Co. KGaA, Weinheim

provide an unambiguous indication to distinguish between the genuine response and the artifacts. Furthermore, refining the measurement configuration is typically a cumbersome and time-consuming process which requires iterative changes on both bias light and bias voltage. In practice, it becomes especially difficult when more than two subcells are involved and/or when the EQE spectra of the subcells spectrally overlap to a great extent, that is usually the case in thin-film silicon-based solar cells.[3,16–20] Similar challenges can also be expected when studying two-terminal multijunction solar cells with novel materials and/or structures, for which the EQEs of the component subcells may not be well-known. In these cases, it can be tricky to determine a proper bias configuration and to interpret the result. This issue is worth extra attention considering that many novel hybrid structures have emerged in the last few years, such as perovskite/crystalline silicon tandem cells,[21–23] perovskite/copper indium gallium selenide (CIGS) tandem cells[24,25] and a-Si:H/organic double- and triple-junction cells.[26] While the researches demonstrated promising routes to surpass the high efficiencies given by optimized single-junction cells, little concern was shown for the credibility of the EQEs being reported.

In experiments, measurement artifacts can be studied by varying the measurement conditions and with different solar cells. The information is quite limited since the current in external circuit is the only output signal. In consequence, understanding the mechanism of artifact formation is not a straightforward task. In this work, we studied the formation of various types of artifact in the EQE measurement of two-terminal multijunction cells by means of modeling. The signal obtained in an EQE measurement of a multijunction cell under defined bias light and bias voltage condition can be simulated. Through the simulations, it was clearly shown how the cell properties or the bias conditions can affect the EQE spectra acquired in measurements. Modeling the entire measurement process gives extra internal information about the operation conditions of the subcells, which leads to better understanding of the mechanisms of artifact formation. The model was also applied to interpret the irregular EQE spectra obtained in actual measurements. The insights gained from the in-depth analyses on artifact formations, together with the application of auxiliary modeling in the measurement and interpretation process, enable more reliable determination of the studied spectral response of multijunction solar cells.

2. Terminology and Scope

In this paper, a measurement artifact means a deviation of the probed EQE from the genuine EQE. The genuine EQE is regarded as an inherent property of the solar cell (and its subcells). We define the genuine EQE as the EQE of a subcell when it operates in its own short-circuit condition and when its parent multijunction cell is under an incident spectrum comparable to the AM1.5G. In contrast, the probed EQE is regarded as a quantity obtained in a measurement. The probed EQE is derived from the detected signal so it is dependent on the measurement condition. It does not necessarily reproduce the genuine EQE, which one intends to measure. The discrepancy between the genuine and probed EQE, i.e., the artifact, is the main object of this study.

Besides, a few terms used in this paper might not be common in literature so they require clear definitions. In principle, the EQEs of different subcells in a multijunction cell are measured separately. In a certain measurement, one sets up a bias condition, which is a combination of bias light and bias voltage, with the intention to measure a certain subcell. To clarify, we refer this subcell being intentionally investigated to as the targeted subcell; the rest of the subcell(s) is referred to as the nontargeted subcell(s). While the incident continuous light is referred to as the bias light, the chopped monochromatic light being used to excite a periodic signal is referred to as the probe light. When the J–V characteristic of a subcell is examined as it is a separate solar cell with its own electrical terminals, such J–V characteristic is referred to as the implied J–V characteristic because it is not accessible in experiments but only in simulations. Similarly, the incident light generates excess carriers in a subcell, which would result in a certain photocurrent if it was an independent solar cell. Because the actual current in a subcell also relies on the other subcells in the series, such hypothetical photocurrent is referred to as the potential photocurrent of the subcell. For simplicity, the potential photocurrent density is indicated as J_{ph}. J_{ph} is also used to quantitatively represent the illumination level of a subcell. Finally, in many cases, a multijunction cell and its subcells are examined at their operation points. The operation point of a (sub)cell is represented by its operation voltage and operation current density (V, J), under a given external condition. An operation point can typically be indicated as a point on the (implied) J–V curve. At such point on the curve, the derivative of current density (J) with respect to voltage (V), dJ/dV, can be examined for further analyses. The derivative is the differential conductance per unit area of the subcell, and is referred to as differential conductance in this paper for simplicity.

This article is structured as the following. With the help of modeling, the mechanisms of artifact formation are analyzed in Section 3. Measurements on tandem solar cells, which are the simplest multijunction cells, have been simulated. The shunt resistance of the targeted subcell, the bias light intensity and the bias voltage were altered to examine how they affect the probed EQE. In Section 3.4, a set of experimentally measured EQE spectra for a quadruple-junction solar cell is shown to demonstrate how modeling can help to interpret the results from actual measurements. Having gained a better understanding of the principle and mechanism behind the EQE measurement and its artifact formation, in Section 4 we gave an in-depth discussion on how to properly conduct the measurement and interpret the outcome. Finally, perspectives are presented in Section 5 on the potential applications of the model. All experimental details regarding the acquisition of simulation input and the demonstrated measurements are reported in Section 7, after the conclusions.

3. Artifact Analysis

In this section, modeling of EQE measurements on multijunction cells is used to study the formation of artifacts. Illustrated in **Figure 1**, a model was developed to simulate the probed EQE of a two-terminal multijunction cell in a differential spectral

© 2016 The Authors. Published by WILEY-VCH Verlag GmbH & Co. KGaA, Weinheim

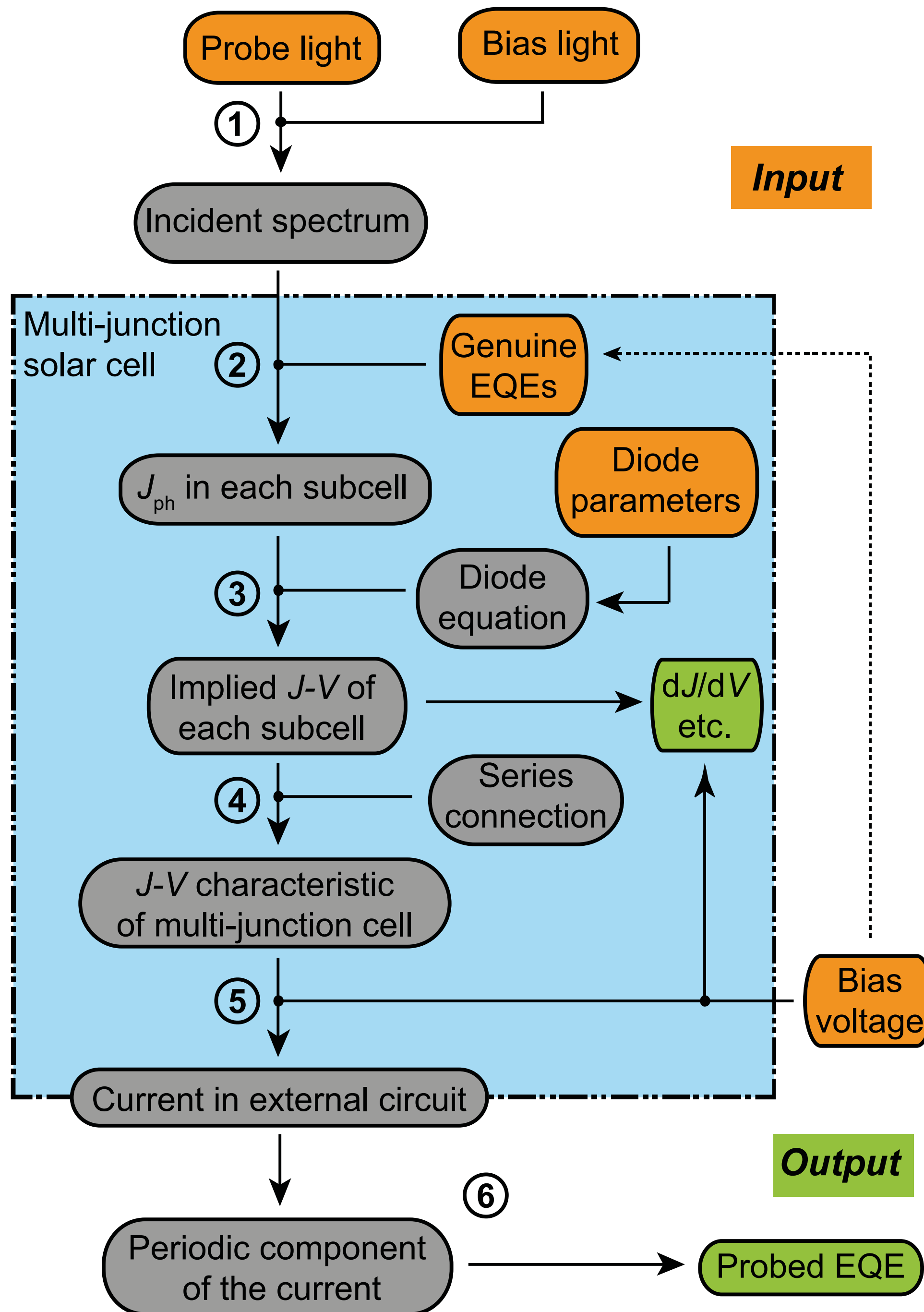

Figure 1. Flowchart of the model simulating the probed EQE of a two-terminal multijunction solar cell under certain measurement configurations. The blue outlined region distinguishes the internal properties of the cell from the external excitation and outcome. The input and output of the model are labeled in orange and green, respectively. The dashed line indicates the extensibility of the model by incorporating additional physical models.

response measurement, in response to a defined measurement condition. The multijunction cell is simulated as a perfect series connection of the component subcells, each of which is approximated by the well-known one-diode equivalent circuit

$$J_i = J_{0_i}\left[e^{\frac{q(V_i - J_i R_{s_i})}{nkT}-1}\right] - J_{\mathrm{ph}_i} + \frac{V_i - J_i R_{s_i}}{R_{\mathrm{sh}_i}} \quad (1)$$

where q, k, and T are elementary charge, Boltzmann constant, and absolute temperature, respectively. The adjustable parameters in the equation J_0, n, R_s, R_{sh} and J_{ph} are the saturation current density, diode ideality factor, series resistance, shunt resistance, and (potential) photocurrent density, respectively. The subscript ($_i$) indicates a certain subcell. Further details of the model are described in the Supporting Information. A complete set of input includes the incident spectra of the bias

© 2016 The Authors. Published by WILEY-VCH Verlag GmbH & Co. KGaA, Weinheim

light and probe light, as well as the genuine EQE and the diode parameters of each subcell. Depending on the purpose of the simulations, the input parameters can be either measured experimentally, synthesized by other simulations, or generated artificially. The ultimate output of the model is the probed EQE with respect to the cell properties and measurement conditions given in the input. In addition to this, the operation points of the subcells and the related information, which cannot be obtained in a measurement, are also valuable output.

Taking into account the device characteristics and measurement condition, the model reflects the realistic response of the device. In the following subsections, several sources of measurement artifacts have been studied by changing the input of the model. Because of the way how the model is constructed, the revealed artifacts are the consequence of the characteristics of illuminated semiconductor diodes (i.e., the subcells) and the correlation between them. The discussions are generically applicable to different types of two-terminal multijunction cells, even though thin-film silicon solar cells were used in the demonstration.

3.1. Effect of Shunt Resistance

EQE measurements of thin-film a-Si:H/nc-Si:H tandem solar cells were simulated to show the influence of shunt resistance of the targeted subcell on measurement artifacts. Without losing genericity, the bottom subcell is chosen as the targeted subcell in the following investigation. In the simulations, R_{sh} of the bottom subcell was adjusted between 200 and 5000 Ω cm^2. The J_{ph} in the bottom subcell generated by the bias light was set at 14 mA cm^{-2}, near its value under AM1.5G illumination. For the top subcell it was set at 20 mA cm^{-2} to guarantee the device current-limited by the bottom subcell. The J_{ph} generated by the probe light was in the order of 10^{-1} mA cm^{-2}. In all cases the bias voltage was 0 V.

Except the R_{sh} of the bottom subcell, the diode parameters of the simulated subcells were kept unchanged at their default values, which are listed in **Table 1**. At the regime where the illumination level is comparable to that under AM1.5G, all diode parameters except J_{ph} can be treated as constants, which were obtained by fitting the one-diode equation with the AM1.5G-illuminated J–V data.

Figure 2a shows the simulated EQE spectra in which artifacts can be observed. In the wavelength range where the bottom subcell has a higher response than the top subcell, the simulated probed EQE is lower than its genuine value; the opposite is true at the wavelengths where the bottom subcell has a lower response. The lower the shunt resistance, the more the probed EQE deviates from the genuine value. Meusel et al. ascribed this kind of artifact to the drift of operation voltage occurring in the subcells stimulated by the probe light.[6] Such mechanism is also explained and further investigated in the Supporting Information with two distinctive examples. In our case, the deviation in current thus the EQE is directly related to the shift of operation voltage in the bottom subcell. The drift is more severe with lower R_{sh}, as it is shown in Figure 2b.

The differential conductance of the subcell at its operation point, which is the slope (dJ/dV) of its implied J–V curve, was investigated as it represents how sensitive the current is to a change in voltage. Figure 2c shows that for the bottom subcell, dJ/dV clearly increased when R_{sh} was reduced. As a result, a subcell with lower R_{sh} suffers from more current drift (ΔJ) in case of a certain voltage drift (ΔV), hence greater extent of artifact. Looking into the operation point of the top subcell, it affects the artifact through different ways at the two wavelengths discussed in the following. At 820 nm, the effect is determined by ΔV in the top subcell induced by the increase in photocurrent, so the artifact is directly affected by dJ/dV at the operation point. It can be seen in Figure 2b,c that ΔV is in line with the variation of dJ/dV in the top subcell. A very steep slope helps to suppress artifacts suggesting that the nontargeted subcell(s) should operate as near its open-circuit point as possible. On the other side, at 460 nm, the mechanism is less straightforward. The ΔV in the top subcell depends on how much its implied J–V curve expands in response to the photocurrent generated by the probe light. Qualitatively, such influence on operation voltage is more pronounced when dJ/dV at operation point is low. Therefore, the requirement at 460 nm conforms to that at 820 nm. In brief, a low dJ/dV for the targeted subcell and a high dJ/dV for the nontargeted subcell(s) are beneficial to the EQE measurement of multijunction solar cells.

The shunt resistance of the targeted subcell affects the measurement artifacts not only through dJ/dV of the implied J–V curve in the reverse voltage regime, but also by locating the operation point of the nontargeted subcell along its implied J–V curve. Figure 2d shows the implied J–V curves of the subcells under only bias illumination. Without bias voltage, the nontargeted subcell typically operates at a positive voltage near its V_{OC}. The targeted subcell works at the corresponding negative voltage, and its operation current determines the current in the device. In the regime of the negative voltage, the operation current highly depends on R_{sh}, even though the potential photocurrents (at 0 V) are the same. As a result, given the same level of bias illumination, a lower R_{sh} in the targeted subcell moves the operation point of the nontargeted subcell toward lower voltage, at which the measurement is more susceptible to artifacts. In other words, an intense bias light for the nontargeted subcell is needed for an accurate measurement in case of a low R_{sh} in the targeted subcell. It can be seen in Figure 2d that, although the photocurrent provided by the probe light was only in the order of 10^{-1} mA cm^{-2}, a difference of 6 mA cm^{-2} in J_{ph} generated by the bias light may not be enough to suppress the artifact when the shunt resistance is low. The configuration of the bias light is not as simple as fulfilling the basic current-limiting requirement (a difference in J_{ph}). Under reverse voltage, the operation current of the targeted subcell may approach or even surpass the J_{ph} in the nontargeted subcell in case of a low R_{sh}. A similar problem can occur when the breakdown voltage of the targeted subcell is low.

Table 1. Default parameters used in the one-diode equation for the demonstrated a-Si:H/nc-Si:H tandem solar cell.

	J_0 [mA cm^{-2}]	n	R_s [Ω cm^2]	R_{sh} [Ω cm^2]
Top subcell	1.05×10^{-8}	1.69	0.94	1000
Bottom subcell	1.05×10^{-5}	1.44	0.65	750

© 2016 The Authors. Published by WILEY-VCH Verlag GmbH & Co. KGaA, Weinheim

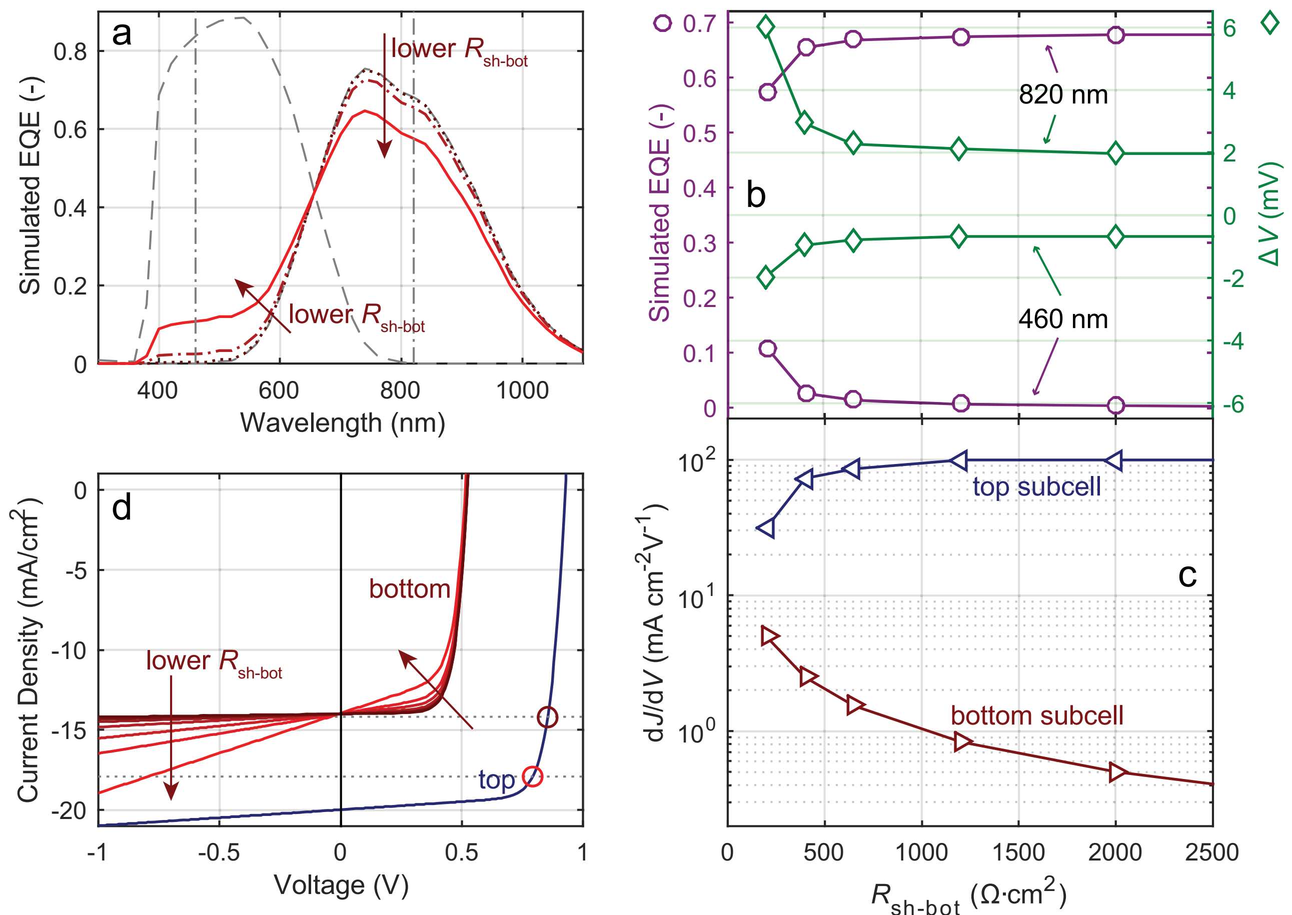

Figure 2. The effect of R_{sh} of the targeted subcell on the EQE measurements. a) The measurement artifact becomes more obvious when R_{sh} is changed in the sequence of 2000, 400, and 200 Ω cm^2. The gray dashed curves show the genuine EQE spectra of the top and bottom subcells,[27] and the vertical dashed-dotted lines indicate the two wavelengths at which the cell operation is further discussed. b) Left axis, circle marker: the probed EQE at certain wavelengths. Right axis, diamond marker: the difference in operation voltage of the bottom subcell between the bias/bias+probe light conditions. c) dJ/dV of implied J–V curves of the subcells at their operation points under only bias light. d) Implied J–V curves of the component subcells under the same bias light condition, but with varied R_{sh} in the bottom subcell. The dotted lines indicate the operation currents of the cells with the highest and lowest R_{sh}. The circles emphasize the different dJ/dV in the top subcell at the corresponding operation points.

3.2. Effect of Bias Conditions

This section reports the effect of the bias-light intensity and of the bias voltage on the measurement artifacts. First, the influence of bias-light intensity was examined. With the bottom subcell as the targeted subcell, its J_{ph} supplied by bias light was assigned at 14 mA cm^{-2}, and the illumination level for the top subcell was changed between 15 and 40 mA cm^{-2}. Similarly to that in Section 3.1, EQE measurements of the tandem cell were simulated using the diode parameters given in Table 1, except the R_{sh} of the bottom subcell was set at a relatively low value of 200 Ω cm^2. The bias voltage is 0 V. **Figure 3**a shows that the probed EQE is substantially different at various illumination level for the top subcell, according to simulations. At the lowest illumination level, that $J_{ph\text{-}top}/J_{ph\text{-}bot}$ = 15/14 mA cm^{-2}, the probed EQE behaves like the EQE of the top subcell with some artifact, even though the J_{ph} in the top subcell is still higher and one may expect a probed EQE representing the response of the bottom subcell.

To understand this phenomenon, the operation points of the subcells are examined in Figure 3b. When the top subcell is supplied a low J_{ph} of 15 mA cm^{-2}, it operates at a low positive voltage near 0 V, instead of the desired high voltage which is near the V_{OC}. In such condition, the top subcell is the one actually throttling the current. The bottom subcell can support the increase in current when an additional potential photocurrent is generated in the top subcell by the probe light, while the opposite is not true. The external current, hence the probed EQE, is more related to the spectral response of the top subcell.

The different profiles of the probed EQE spectra can be explained by the differential conductance dJ/dV of the component subcells at their operation points, as shown in Figure 3c. At the highest illumination level, dJ/dV of the top subcell is higher than that of the bottom subcell by more than one order of magnitude. The probed EQE aligns well with the genuine EQE of the bottom subcell. When the difference between the dJ/dV of the two subcells decreases, the probed EQE deviates more from the genuine EQE of the bottom subcell. The

© 2016 The Authors. Published by WILEY-VCH Verlag GmbH & Co. KGaA, Weinheim

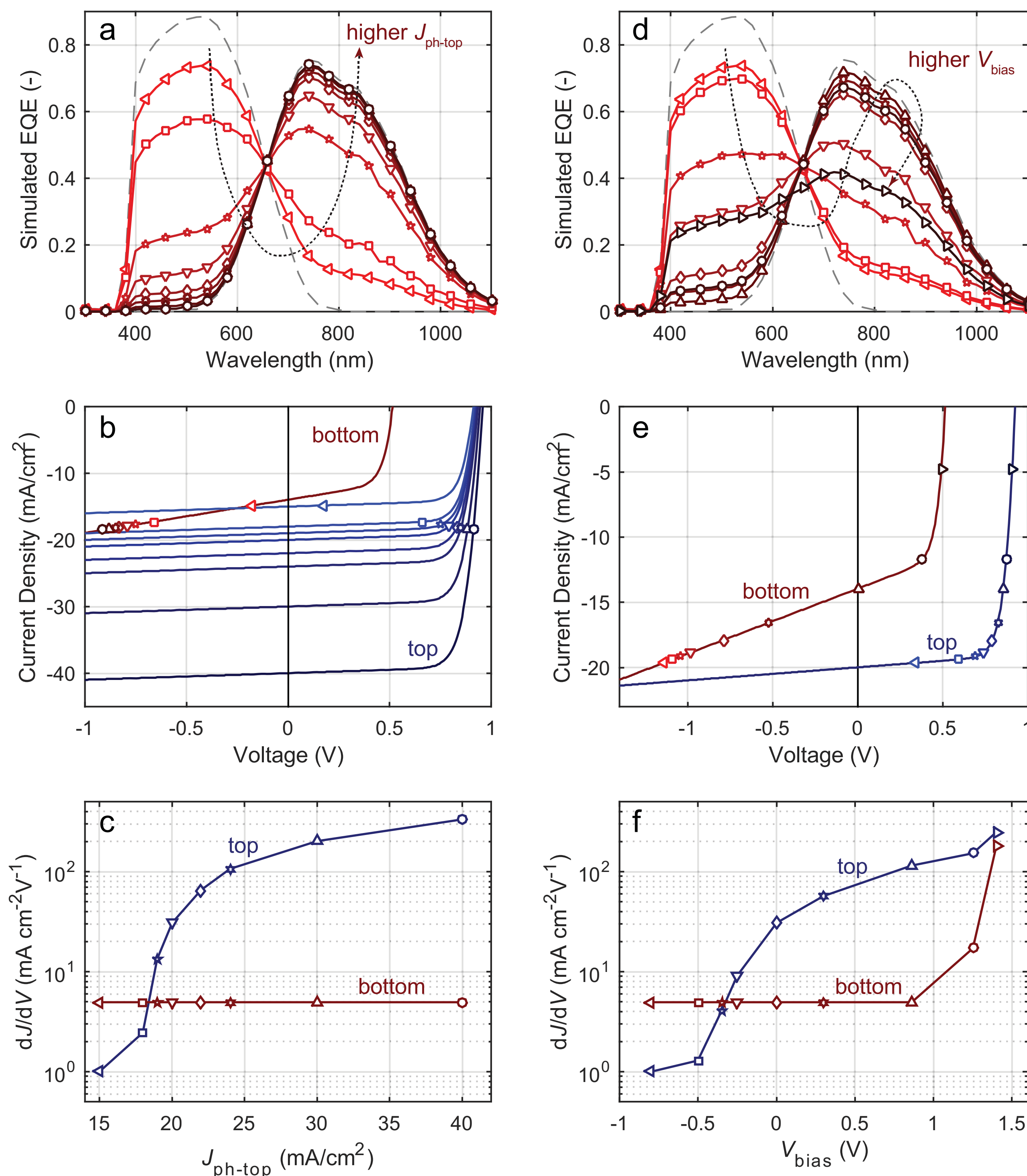

Figure 3. Illustration of how the bias light or bias voltage affects measurement artifacts. a–c) Simulations of EQE measurements with different bias illumination levels in the nontargeted subcell. The probed EQE spectra in panel (a) show the evolution of artifacts with the intensity of the bias light. b) Implied *J*–*V* curves of the subcells under certain bias light conditions, with the markers indicating the operation points. c) d*J*/d*V* at the operation points under different bias light levels J_{ph-top}. d–f) Simulations of EQE measurements with different bias voltage applied. Note that in panel (d) the probed EQE changes with V_{bias} in different ways in two different voltage regimes.

trend continues until a point where d*J*/d*V* of the top subcell goes lower than that of the bottom subcell. In those illumination conditions, the probed EQE exhibits like the EQE of the top subcell. Therefore, Figure 3a–c explains how a high illumination level for the nontargeted subcell can mitigate the artifacts. By increasing the illumination level J_{ph} in the

© 2016 The Authors. Published by WILEY-VCH Verlag GmbH & Co. KGaA, Weinheim

nontargeted subcell, its operation voltage is positioned toward its V_{OC}, around which the nontargeted subcell has the steepest $J–V$ relation thus interferes the least with the external current and the probed EQE.

Figure 3a,c reveals that the lower the dJ/dV of a certain subcell at its operation point, the greater weight the genuine EQE of this subcell has on the probed EQE. This claim can be justified by the nature of dJ/dV, which can be interpreted as the differential conductance of the subcell at the operation point. At the operation point, when a subcell has a very high differential conductance, the subcell works like a conductor that it hardly affects the current running through the device. Consequently, a subcell with high dJ/dV contributes very little to the probed EQE. In contrast, a subcell with a very low differential conductance is highly resistive such that it limits the current. As a result, the probed EQE is dominated by the subcell with the lowest dJ/dV at the operation point.

In terms of alleviating measurement artifacts, the configuration of bias voltage (V_{bias}) could also play a big role considering its relevance to the operation points. Looking into this issue, EQE measurements of a tandem solar cell were simulated with V_{bias} being tuned from –0.8 to +1.4 V. Once again, R_{sh} of the bottom subcell was set at 200 Ω cm^2 to make the artifacts more noticeable, while the other diode parameters were kept the same. With the bottom subcell being the targeted one, the bias illumination level was fixed at $J_{ph\text{-}top}/J_{ph\text{-}bot}$ = 20/14 mA cm^{-2}. Under the bias light, the V_{OC} of the top subcell is 0.93 V.

A trend similar to the effect of bias illumination can be seen in Figure 3d–f when V_{bias} ranging between –0.8 and +0.86 V. In this range, the differential conductance dJ/dV of the bottom subcell at its operation point is constant while the one of the top subcell increases with V_{bias}, leading to a transition of the probed EQE from a top-subcell-like response to a bottom-subcell-like response. With V_{bias} surpassing +0.86 V, at which the operation voltage of the bottom subcell equals 0 V, dJ/dV of the bottom subcell rises abruptly with V_{bias}. It corresponds to the region in which the bottom subcell operates at positive voltage and its operation current becomes more sensitive to the change in operation voltage. As a consequence, the transition of probed EQE with increasing V_{bias} is reversed. The influence from the top subcell becomes significant at high voltage. This phenomenon can be expected from Figure 3f since the difference between the dJ/dV of the two subcells deminishes in the high-voltage regime.

Commonly, applying a positive bias voltage is taken as a measure to compensate the voltage offset from the nontargeted subcells with the aim that the targeted subcell can be examined near its short-circuit condition. Here, we demonstrated that even without taking in account the possible voltage-dependent photoresponse of the targeted subcell, an appropriate bias voltage is still beneficial solely because of the illuminated $J–V$ characteristics of the nontargeted subcells, that is, the diode-like $J–V$ response exhibits a greater dJ/dV at a higher operation voltage. It is noteworthy that beyond a certain limit the positive bias voltage turns to be detrimental. In the shown example the optimal bias voltage was slightly lower than the V_{OC} of the nontargeted subcell. However, finding the optimum is not always as easy when the number of subcells increases and/or the bias illumination level is distinct from the standard testing condition.

3.3. Illumination-Dependent Response

3.3.1. Adapted Model for Low-Light Regime

The capability of our model to reproduce measurement artifacts is decided by the effectiveness of the assumptions and physical equations used in the model for describing the behavior of the studied multijunction cells. One should always bear in mind the conditions in which a model is (relatively) valid. The results discussed in the previous sections are based on the one-diode equivalent circuit. Such model is very useful for identifying the artifacts raised by the diode-like $J–V$ characteristics in general photovoltaic cells at an illumination level comparable to AM1.5G, which is the case in Sections 3.1 and 3.2. On the other hand, the diode parameters acquired at a certain illumination level do not guarantee a good match with the $J–V$ data obtained in a different condition. An EQE measurement of a tandem cell in dark condition (no bias light) was simulated using the parameters obtained from illuminated diodes. The simulated probed EQE shown in **Figure 4**a (the curve labeled "w/o adaption") gives a broad spread over the spectrum. On the contrary, it is commonly expected and often observed that the EQE measured in the dark mainly outlines the overlap between the EQE spectra of all component subcells. Although such expectation was not always met as shown in literature,[7,28,29] the result in Figure 4a is worth extra attention. In this case, the discrepancy between this simulation and the aforementioned expectation originates from a shunt leakage overestimated by the parameters of illuminated diodes. It can be explained by the measured $J–V$ curves of an a-Si:H single-junction cell under dark and AM1.5G conditions, respectively. This exact cell is the one used to acquire the diode parameters of the top subcell in the demonstrated tandem cell. For better comparison of their reverse characteristics, the illuminated $J–V$ curve in Figure 4b is shifted so that it comes across the origin. Apparently, the short-circuit resistance ($[dJ/dV]^{-1}$ at $V = 0$ V) of the dark $J–V$ curve is much higher than that of the illuminated one, meaning that the change in current caused by a voltage drift is smaller in the dark case. Therefore, the use of the diode parameters acquired from the $J–V$ relation measured under AM1.5G spectrum overestimates the shunt leakage in the dark and low-light conditions. Generally speaking, such behavior can happen when the impedance of the solar cell is not a constant but can be affected by the carrier concentration or injection level in the cell. In case of solar cells constituted by P-I-N diodes, such change of impedance in the short-circuit region can be caused by the recombination losses in the intrinsic layer which are dependent on the carrier concentration thus also on the J_{ph}.[30]

The model used in the previous sections was adapted to extend the applicable range over low-light conditions. The one-diode equivalent circuit was kept for synthesizing the $J–V$ relation, but the diode parameters were interpolated between their dark and AM1.5G-illuminated values. When the one-diode equation was individually fitted with the two $J–V$ curves in a pair, such as the two solid lines shown in Figure 4b, it was found that the diode parameters mainly differed in R_{sh} besides J_{ph}. Therefore, a semiempirical approach inspired by the work of Merten et al.[30] was used for the interpolation of R_{sh}. Assuming a linear relation between log R_{sh} and log J_{ph}, the R_{sh}

© 2016 The Authors. Published by WILEY-VCH Verlag GmbH & Co. KGaA, Weinheim

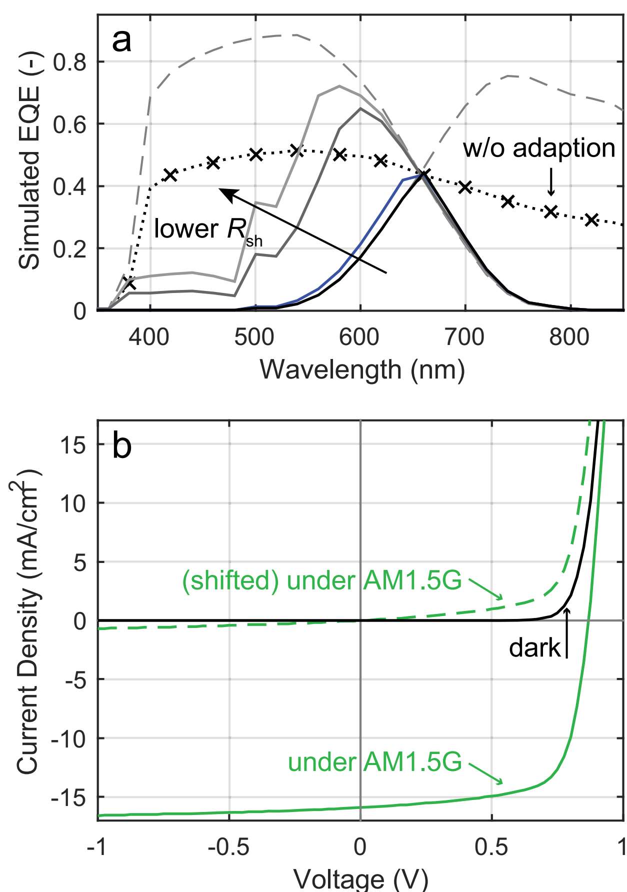

Figure 4. The response of solar cells in the dark and illuminated conditions cannot be described with the same set of one-diode parameters. a) Simulations of EQE measurement on tandem cells in the dark condition. The dotted line with cross markers was simulated with the diode parameters acquired under AM1.5G spectrum. The solid lines were simulated using the adapted model with different R_{sh} in the bottom subcell. The blue line is from the reference cell. The dashed lines are the genuine EQE of the top and bottom subcells. b) Experimentally measured *J–V* curves of a single-junction a-Si:H cell under dark and AM1.5G-illuminated conditions. The illuminated one is also shifted and aligned to the origin, plotted as a dashed line, for more straightforward comparison.

at a certain illumination level J_{ph} was interpolated between the two known data points from the dark and AM1.5G conditions.

For the sake of model validation, measurements of the same tandem cell in the dark condition were simulated with the adapted model. The parameters in Table 1 were used for both dark and AM1.5G-illuminated conditions, except the dark R_{sh} was both set at 6.7×10^5 Ω cm^2 based on the measured dark *J–V* data. The AM1.5G-illuminated J_{ph} was 14.0 and 28.0 mA cm^{-2} for the top and bottom subcells, respectively, while the dark J_{ph} was 0.002 mA cm^{-2} for both. This diode configuration is based on the measurements on the fabricated cells, and it serves as the reference cell in the following study.

The simulation output of the adapted model is shown in Figure 4a. For the reference cell, the EQE probed in the dark basically follows the overlap of two genuine EQE spectra with a slight increase. The slight deviation is not a fault of the simulation but a realistic indication of the shunt leakage at such illumination level. To demonstrate this, the influence of shunt leakage was further examined by simulating tandem cells with different R_{sh} in the bottom subcell. In this series of simulations, the reference $R_{sh\text{-}dark}$ and $R_{sh\text{-}AM1.5G}$ of the bottom subcell were multiplied by factors of 1/50, 1/25, 50, and 1/10, 1/5, 10, respectively. The result is shown in Figure 4a along with the reference one. For the cell with extremely high R_{sh} in the bottom subcell, the probed EQE strictly follow the genuine EQE of the bottom subcell in the wavelengths where the top subcell has a higher genuine EQE. When R_{sh} of the bottom subcell decreases, the probed EQE tends to present the spectral response of the top subcell, showing that the bottom subcell with low R_{sh} cannot properly limit the current in the device. This qualitative demonstration agrees with the trend reported by Pravettoni et al. and Bahro et al.[7,28] With such adaption the model was greatly improved and specialized for simulating thin-film silicon solar cells, and can be applied to analyze the measurements conducted in the low-light regime.

3.3.2. Effect of Low Bias Illumination

The effect of low bias illumination on the EQE measurement was investigated by implementing the adapted model. The reference tandem solar cell was simulated with the bottom subcell being the targeted subcell. The bias light for the top subcell was set at a high level of $J_{ph\text{-}top}$ = 20 mA cm^{-2} in order to isolate the studied effect from other influences. The bias light for the bottom subcell was varied in a wide range: $J_{ph\text{-}bot} = 1.4 \times 10^{-4}$–$1.4 \times 10^1$ mA cm^{-2}. In all cases, the potential photocurrent generated in the top subcell was much higher than that in the bottom subcell. The probed EQE at zero V_{bias} is plotted in **Figure 5**a. This series of EQE spectra exhibits very different features from the ones shown in the previous sections. First, there is barely any artifact signal at the wavelengths that the bottom subcell has zero genuine EQE. It is due to the intense light saturation in the top subcell that effectively prevents any artifacts caused by a voltage drift. Second, the probed EQE is higher than the genuine one. The enhancement in probed EQE increases monotonically with the decrease in $J_{ph\text{-}bot}$ generated by bias light. This type of artifact can be ascribed to the illumination-dependent *J–V* characteristics of the targeted subcell.

To explain this type of artifact, in Figure 5b the implied *J–V* curves of the bottom subcell were examined with and without the probe light at 820 nm, the wavelength at which the top subcell is not active. In this low-light scenario, the bias-induced $J_{ph\text{-}bot}$ is 1.4×10^{-2} mA cm^{-2}, while at this wavelength the used monochromatic probe light generates a $J_{ph\text{-}bot}$ of 0.2 mA cm^{-2}. The difference in the currents at short-circuit points between the two *J–V* curves is the J_{ph} supplied by the probe light thus directly related to the genuine EQE, while the corresponding difference at operation points decides the probed EQE. The R_{sh} in the two conditions are largely different, leading to different slopes between the two *J–V* curves in their reverse-voltage regime. In consequence, the difference in the currents at operation points is enhanced from that at short-circuit points. A probed signal higher than the genuine EQE is formed, seeming an artifact.

© 2016 The Authors. Published by WILEY-VCH Verlag GmbH & Co. KGaA, Weinheim

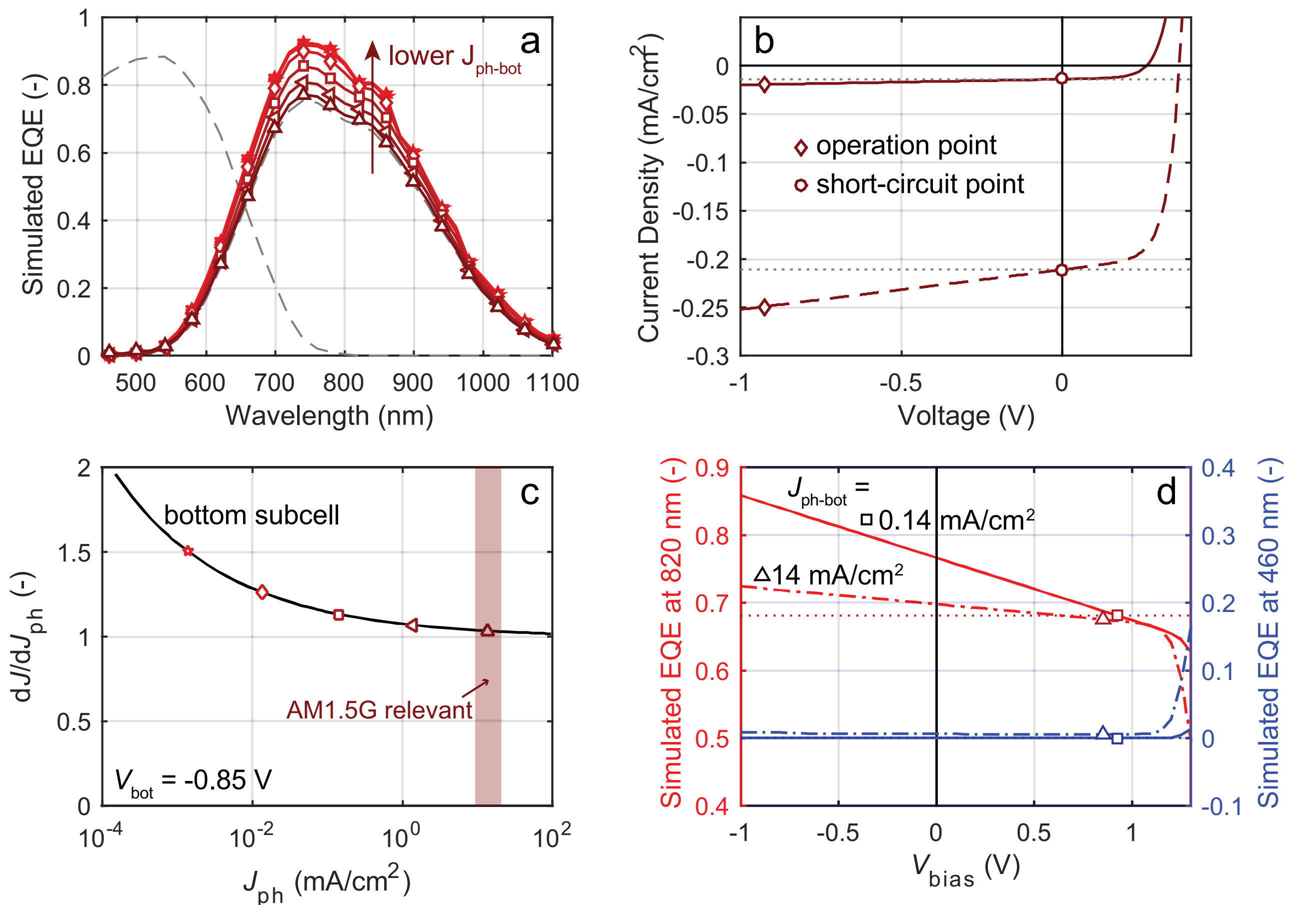

Figure 5. The probed EQE depends on the illumination level for the targeted subcell. a) Probed EQE simulated with various bias illumination levels for the bottom subcell. The dashed lines show the genuine EQE of the two subcells. b) Implied J–V curves of the bottom subcell without (solid line) and with (dashed line) 820 nm probe light, with the markers indicating the operation points and the short-circuit points. The dotted lines indicate the two J_{ph} levels. c) The variation rate of the operation current of the bottom subcell at an operation voltage of −0.85 V, in response to the variation of J_{ph}. d) Probed EQE simulated at 460 nm (blue) and 820 nm (red) in two different illumination levels. On each line a marker is placed at the point where the operation voltage of the targeted subcell is 0 V. The markers representing the illumination level are consistent across (a)–(d).

The probed EQE is subject to the illumination level as seen in Figure 5a. The dependency originates from the principle of differential spectral response measurement, that the output signal is not the total current through the device over the total incident light, but the periodic component of the current, divided by the incoming chopped monochromatic light. In other words, the probed EQE depends on how fiercely the J–V characteristic changes with the additional incident light, at the particular illumination level. As an example, the bottom subcell in the adapted model was analyzed to assess how sensitive the operation current density is to J_{ph}. Such sensitivity was evaluated by dJ/dJ_{ph}, the derivative of the operation current density with respect to the potential photocurrent density. Examined at an operation voltage of −0.85 V, in Figure 5c the derivative is shown against the illumination level J_{ph}. Clearly, dJ/dJ_{ph} is not uniform throughout the inspected scope of illumination. Ideally, it equals 1 so the probed EQE matches the genuine EQE. Instead, its value is almost 2 in the darkest condition, and converges toward 1 in the high-illumination regime. It is the exact root of the varying signals in Figure 5a.

In the simulations, the dependency of dJ/dJ_{ph} on J_{ph} is a direct consequence of the way how R_{sh} is interpolated in the adapted model. In actual measurements on a variety of multijunction cells fabricated in different photovoltaic technologies, the cause of illumination-dependent response can be diverse. In general, a similar behavior can be expected whenever such derivative of operation current in the targeted subcell is not uniform over the relevant illumination range. This phenomenon illustrates the need of bias light even for the targeted subcell. Since the probed EQE is correlated with the amount of continuous J_{ph} in the subcell, the targeted subcell should be biased at an illumination level close to its intended operation condition, as commonly suggested.[15]

In fact, in spite of the variance, the probed EQE spectra shown in Figure 5a do not contain much artifacts, but rather represent the EQE of the subcell at certain operation conditions, namely, under low bias light and negative operation voltage. The bias-light and bias-voltage dependences of EQE are not exclusive in the multijunction cells but are rather common phenomena in single-junction cells.[31]

© 2016 The Authors. Published by WILEY-VCH Verlag GmbH & Co. KGaA, Weinheim

Conventionally, the EQE of the subcell under an illumination near solar irradiation and at the short-circuit point is the main concern and was mostly reported. For that, a positive bias voltage is usually applied to compensate the voltage contribution from the nontargeted subcell(s) and to shift the operation point of the targeted subcell to the desired voltage. Figure 5d shows the effect of the bias voltage under two different illumination levels. When V_{bias} applied to the tandem cell is 0 V, the probed EQE gives different values in the two conditions. The dependency of probed EQE on V_{bias} is more obvious in case of low $J_{ph\text{-}bot}$, except for very high V_{bias}. By applying a V_{bias} equal to the operation voltage of the top subcell, the bottom subcell operates in the vicinity of 0 V, so the genuine EQE can be approached in both scenarios (For $J_{ph\text{-}bot} = 14$ mA cm^{-2}, there is a slight artifact because of the voltage drift in the top subcell). From the view point of actual measurements, however, it also means that the probed EQE changes continuously with V_{bias} and there is no clear signature to distinguish the optimal V_{bias}. Of course, in the high-voltage regime the probed EQE spectrum is largely distorted on account of both subcells operating at high forward voltages, so the upper limit of V_{bias} can be decided. For a more precise optimization of the bias configuration, further analyses by modeling or additional experiments are required.

3.4. Experimental Application

The purpose of developing the model in this work is to understand the formation of artifacts in EQE measurements so that the artifacts embedded in experimental results can be distinguished from the genuine properties of interest. Tandem solar cells, the multijunction cells which consist of the least component subcells, were studied in the previous sections, because the limited complexity eases the analysis on artifact formation. When there are three or more subcells in a multijunction cell, the internal correlations are complicated with the increased variables in the circuit, while the number of terminal is kept the same at two. In experiments, it becomes difficult to interpret the measurement results solely by adjusting the bias configurations. Nevertheless, the principles of the interactions between the subcells are similar no matter how many of them the multijunction cell comprises. The model can therefore be used for interpreting those intricate experimental results.

As a demonstration of the experimental usage of our model, the model was applied to the measurements of a quadruple-junction thin-film a-SiO$_x$:H/a-Si:H/nc-Si:H/nc-Si:H solar cell. The structure and performance of a similar cell have been reported elsewhere.[18] As a result of the absorber selection and optical design in such devices, the EQE spectra of the subcells strongly overlap with each other in the spectrum, as shown in **Figure 6**a. The measurements on these cells typically feature a demanding process of adjusting the bias light. Besides, it can be observed in the measurement results that not only the intensity but also the spectral profile of the probed EQE can sometimes be changed with varied bias voltage. An example is shown in Figure 6b. During the measurement, the bias light was provided by three light-emitting diodes (LEDs) with emission peaks at the wavelengths of 447.5, 470, and 530 nm, respectively, with the intent to saturate the first, second, and third subcells. The three curves plotted in the figure were measured with a bias voltage of −0.2, +1.4, and +2.4 V, respectively. Comparing to the reference spectra in Figure 6a, at V_{bias} of −0.2 V, the probed EQE looks like what can be expected from the third subcell. In the transition from −0.2 to +1.4 V, the onset of the probed EQE was shifted to the wavelength at which the fourth subcell should start to react. When V_{bias} was further increased, the signal declined in intensity, but extended to the short wavelengths at which the previous two measurements at lower V_{bias} received no response. This kind of evolution is not commonly expected from the adjustment of bias voltage. Incidentally, the discontinuity around 850 nm in all three curves is just an artifact induced by the specific measurement setup.

To explicate the origin of the irregular EQE being observed, simulations of the measurements on this device were performed. Figure 6c,d shows the implied J–V curves of all four component subcells as well as the J–V curve of entire cell, under the illumination of only bias light. It should be noted that the additional part of the J_{ph} generated by probe light is only in the order of 10^{-2} mA cm^{-2} when the subcell has a high response at that wavelength. Therefore, the situation with probe light was not depicted for a better clarity of the graph. The implied J–V characteristics are the core of the dependency on V_{bias} shown in Figure 6b. It can be seen that the fourth subcell has the least J_{ph} under the bias light, followed by the third subcell. The bias-induced J_{ph} in the subcells are, from the first to the fourth, $3.7/1.2/3.7 \times 10^{-1}/1.5 \times 10^{-1}$ mA cm^{-2}. The graph of implied J–V curves can be divided into three regimes, each of which corresponds to a probed EQE spectrum in Figure 6b. In regime (I) where the external bias voltage is at the lower end, the fourth subcell operates at a high reverse voltage supplied by the other subcells. The amplitude of operation current is so high that the third subcell also operates in its low-conductance ($\mathrm{d}J/\mathrm{d}V$) regime. When R_{sh} of the third subcell is higher than that of the fourth subcell, the operation current is throttled by the third subcell so it dominates the probed EQE, as seen in Figure 6b. In regime (II), with a higher V_{bias}, all subcells except the fourth one operate near their V_{OC}, so the probed EQE mainly presents the photoresponse of the fourth subcell. If V_{bias} further increases, the cell is in regime (III) where all the subcells operate near their V_{OC}. The probed EQE contains the influences from all subcells with different weights related to the differential conductance $\mathrm{d}J/\mathrm{d}V$ in the individual subcells at their operation points. As a result, the probed EQE had nonzero values in the wavelength range below 500 nm, where the third and fourth subcells should have zero response.

In the above example, the simulations helped to explain the irregular response observed in experiments, which is the spectrally inhomogeneous dependency of the measured EQE on bias voltage. More importantly, it reflects the capability of the model to identify the sources of the probed EQE obtained in experiments, that is of significant importance in the research and development of two-terminal multijunction solar cells.

4. On the Proper Measurement Configuration and Interpretation

It has been demonstrated so far that the signal collected in a EQE measurement of a two-terminal multijunction cell is

 © 2016 The Authors. Published by WILEY-VCH Verlag GmbH & Co. KGaA, Weinheim

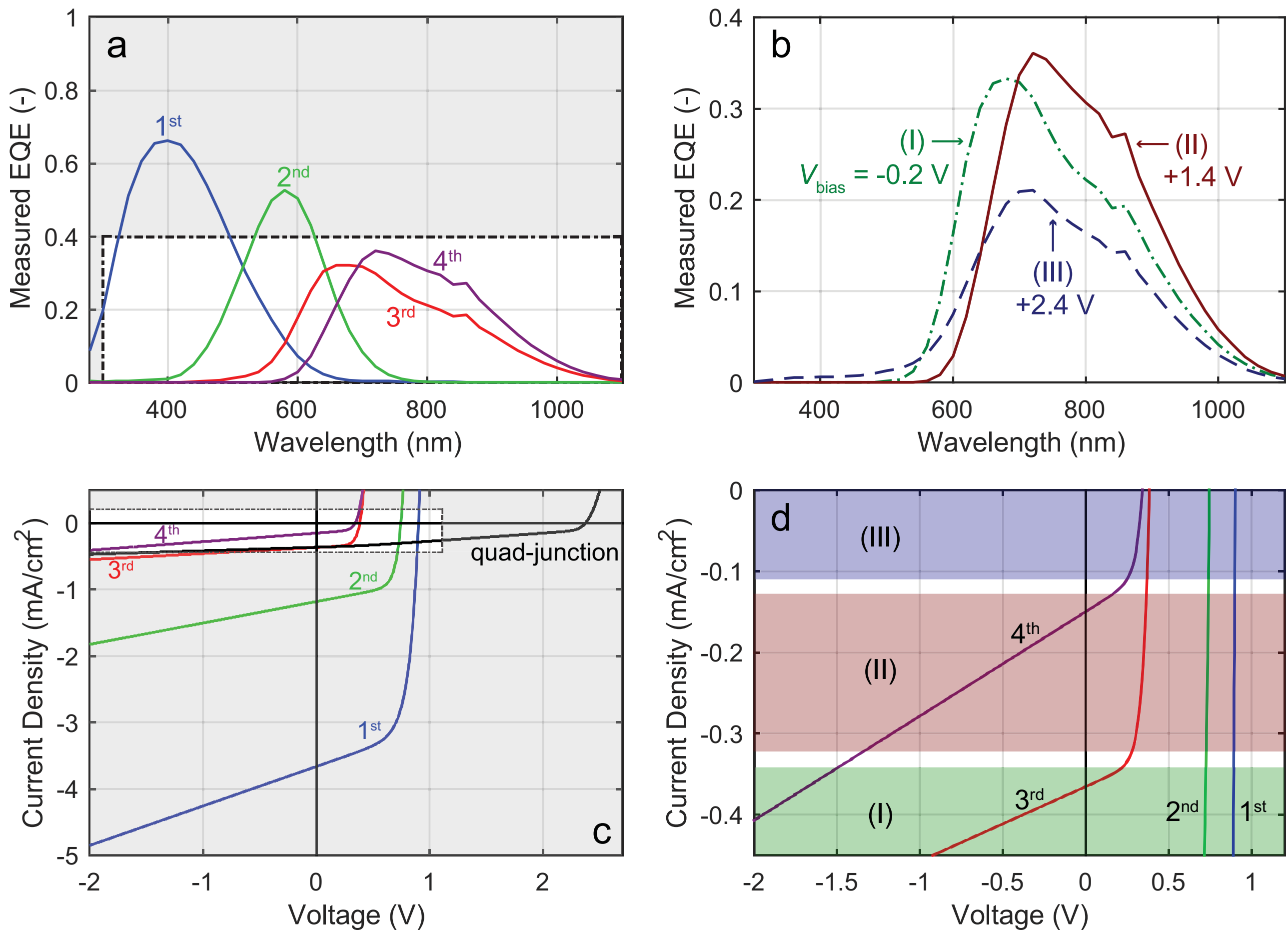

Figure 6. Voltage-dependent EQE measurements of a quadruple-junction cell. a) Genuine EQE spectra of the four component subcells. b) Experimentally measured EQE spectra show different spectral profiles with varied V_{bias} and fixed bias light configuration. Note that the chart has a same scale as the unshaded area in panel (a). c) Simulated *J–V* curve of the quadruple-junction cell, and the implied *J–V* curves of the four component subcells under only bias illumination. d) The unshaded area in panel (c), which is the part more relevant to the cell operation during the measurements. The graph is divided and rendered into three operation regimes corresponding to the three probed spectra in panel (b).

subject to the measurement configuration including the bias light, probe light, and bias voltage. Such dependency originates from the electrical correlations between the component subcells as well as the optoelectrical characteristics of each subcell as an individual photovoltaic device. The configuration of a measurement is inherent not only in the measuring process but also in the data interpretation, of which people are not always aware. Concerning the EQE measurement, there are two natural questions and they should always come as a duo— "What configuration?" and "What does the result mean?"

With regard to single-junction cells, one may think of a few different measurement configurations. In all cases, the bias light should provide an illumination similar to AM1.5G or other interested spectrum, while the intensity of the probe light should be negligible and only result in a perturbation in the current. Depending on the purpose of the measurement, there are a few sensible choices of bias voltage which lead to different interpretations. First, the short-circuit condition that $V_{bias} = 0$ V is the most commonly used. The integration of EQE measured and weighted by the incident spectrum gives the J_{SC} of the cell. Second, the cell can be biased as $V_{bias} = V_{MPP}$ where V_{MPP} is the operation voltage of the cell at its maximum power point. This might be more relevant to the actual operation of a solar cell and shows spectrally how photocarriers are generated and collected under such condition. Finally, in some occasions a V_{bias} of negative value is used to enhance the carrier collection and reduce the recombination losses so that the effective optical absorption can be revealed.

The measurement of two-terminal multijunction cells requires essentially different configurations and interpretations compared to the single-junction. These distinctions deserve more attention than what they have been given. The concepts used in measuring single-junction cells cannot be directly transferred. Setting V_{bias} at 0 V or V_{MPP} of a multijunction cell apparently does not give access to the EQE of its component subcells in their short-circuit or maximum-power-point condition because of the nature of two-terminal structure. Every single measurement is supposed to examine only one of the subcells, and the bias configuration should be designed for it. In terms of bias voltage, $V_{bias} = 0$ V lets the targeted subcell operate at a reverse voltage decided by the other subcells. This effortless setting is clearly not a good option because it is susceptible to

© 2016 The Authors. Published by WILEY-VCH Verlag GmbH & Co. KGaA, Weinheim

artifacts as shown previously, meanwhile, is not related to any relevant operation condition of the multijunction cell.

By applying a certain positive V_{bias}, the EQE of a subcell can be examined at its own short-circuit point. This method was widely reported in literature.[5,6,9,11–15,32,33] On one hand, it gives useful information of how the incident photons can be distributed and utilized in different subcells, thus an important means to obtain the feedback needed for optimizing the cell fabrication and achieving current matching between the subcells. On the other hand, the short-circuit points of the subcells do not correlate with the short-circuit point nor other relevant operation conditions of the whole device under solar irradiation. Many researchers calculated the so-called J_{SC} of the subcells from the EQE spectra obtained by this method, and further assigned the lowest value among these J_{SC} of the subcells as the J_{SC} of the multijunction cell based on the principle of current limitation in a series connection. Such interpretation, however, is not rigorous. The problem is illustrated in **Figure 7**a. This example assumed a tandem cell similar to the ones simulated in the previous sections. The R_{sh} of the top and bottom subcells is at reasonably high value of 1000 and 750 Ω cm², respectively. Under AM1.5G illumination, the top and bottom subcells generate current densities J_{ph} of 14.0 and 14.5 mA cm^{-2}, respectively, at the short-circuit points of their implied J–V curves. Following the conventional approach one may report a J_{SC} of 14.0 mA cm^{-2} based on the measured EQE of the two subcells, but in Figure 7a the J–V curve of the tandem cell shows that the J_{SC} is actually 14.2 mA cm^{-2}. The curves in Figure 7a were simulated according to the assumed J_{ph} of the subcells, and they conform to the requirement of perfect series connection. In case these equations are held in a multijunction cell, it can be mathematically proven that the J_{SC} of the multijunction cell is always greater than the lowest J_{ph} among the component subcells. Therefore, EQE of the subcells measured at their own short-circuit points may not give the J_{SC} of the multijunction cell with satisfactory accuracy, despite the useful information which they deliver.

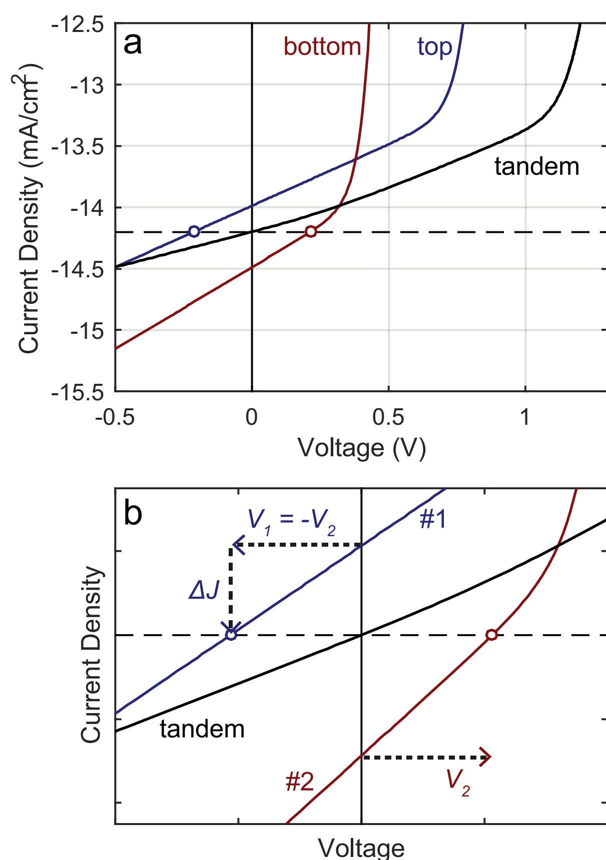

Figure 7. J–V and implied J–V curves of a tandem cell and its component subcells, respectively, under the illumination of AM1.5G spectrum. The dashed line indicates the J_{SC} of the tandem cell. The opened circles on the implied J–V curves show the operation points of the subcells when the tandem cell is in short-circuit condition. a) A specific tandem cell as an example. b) Estimation of the possible discrepancy ΔJ.

To give an estimation of the possible discrepancy, the J–V characteristics of a tandem solar cell are considered. In a tandem cell where the subcell #1 provides less J_{ph} under AM1.5G than the subcell #2 does, as exemplified in Figure 7b, the discrepancy between the J_{SC} of the tandem cell and the lowest J_{ph} among the component subcells is

$$\Delta J \approx V_1 \cdot [dJ/dV]_1 |_{(V=0)} \approx -V_2 \cdot R_{sh_1}^{-1} \quad (2)$$

For a reasonably current-matched tandem solar cell, the practical upper limit of $|\Delta J|$ can be approximated at $V_{MPP2} \cdot R_{sh1}^{-1}$, where V_{MPP2} is the voltage of the maximum power point around which the slope of the implied J–V of subcell #2 changes abruptly. Based on this estimation, if $V_{MPP2} = 0.5$ V, the maximum discrepancy ΔJ is 0.5 and 0.05 mA cm^{-2} for a R_{sh1} of 1 and 10 kΩ cm², respectively. Therefore, the discrepancy in the J_{SC} determined by EQE measurements is not always negligible when the R_{sh} of the subcell is a few kΩ cm² or lower.

When a certain operation condition of a multijunction cell is of interest, the EQE measurement of its component subcells should also be related to such condition. To proceed with the measurements, the determination of measurement configurations should involve multiple steps:

(1) Decide the interested operation condition of the multijunction cell, based on the purpose of the study.
(2) Find the operation condition of the targeted subcell corresponding to the interested operation condition of the multijunction cell. This is the condition in which the subcell should operate during the measurement.
(3) Set up a measurement configuration to fulfill the required operation condition of the targeted subcell, and to properly bias the rest of the subcells at the same time.

For example, to investigate the tandem cell in Figure 7a under AM1.5G illumination and in short-circuit condition, the targeted subcell should be biased to the corresponding operation point indicated in the figure. Measuring the top subcell requires the bias light supplying a J_{ph} of 14.0 mA cm^{-2} for the top subcell and much more for the bottom. The bias voltage should be applied such that the operation voltage of the top subcell is −0.22 V. Accordingly, when measuring the bottom subcell, it should have a J_{ph} of 14.5 mA cm^{-2} and an operation voltage of +0.22 V. Nevertheless, it should be noted that this type of measurement requires extensive knowledge of the

 © 2016 The Authors. Published by WILEY-VCH Verlag GmbH & Co. KGaA, Weinheim

multijunction cell being investigated, which may be obtained by optical and electrical simulations and some preliminary measurements. It might be used for the in-depth analysis of a device, but it is certainly not a means of finding the J_{SC} of a multijunction cell.

Having discussed various possible measurement configurations, it turns out that the spectral response measurement of two-terminal multijunction solar cells cannot be used as a tool to precisely determine the J_{SC}. Instead, the measurement provides a great deal of information about the component subcells, which may then be used to approximate the J_{SC} of the multijunction cell. The accuracy of the estimation can be improved by J–V analysis similar to that in Figure 7.

5. Outlook

Besides the understanding of certain artifacts as an obvious outcome, the motivation of developing such a model in this work is to bring up the awareness of measurement artifacts, so as to promote reliable characterizations and accurate reporting in the field of photovoltaic research. The model was demonstrated with thin-film silicon-based solar cells, but its application is more generic, covering the multijunction cells made with various photovoltaic technologies. As suggested in Figure 1, supplementary physical models can be inserted at different parts in the flowchart to adapt the model to different types of solar cell, so that the specific characteristics related to their constituting materials can be accurately described and simulated. The adaption made in Section 3.3 for describing the illumination-dependent J–V characteristics is an example. Similarly, modifications can be made for the nonlinear J_{SC}-irradiance behavior[34,35] and the photoshunt effect[36] in organic solar cells, or for the luminescence coupling effect[8,37] in solar cells consisting of III–V semiconductors, etc. With such extensibility, the model is useful for the experimental study of two-terminal multijunction solar cells made of novel combinations of absorber materials, and for the cells with unfamiliar or complex spectral response. By simulating the response of solar cells to diverse bias conditions (the preliminary input about spectral response can be generated by optical simulations),[18,32,34] the appropriate measurement configurations can be quickly approached. It is particularly important nowadays considering the emergence of many novel hybrid multijunction structures.

6. Conclusions

Having the incident spectrum and bias voltage to construct a virtual measurement condition, our model proposed a generic way to simulate the internal activities of a two-terminal multijunction solar cell during the process of spectral response measurements. By simulations, sources of artifact formation have been examined. Internally, the influence of shunt resistance in the targeted subcell was confirmed that lower shunt resistance leads to greater voltage drift in other subcell(s) thus more undesirable change to the probed EQE. Externally, the impact of bias conditions was investigated, including the bias-light intensity for the targeted and nontargeted subcells, as well as the bias voltage applied to the two terminals. In brief, the spectral response of the subcell with the lowest differential conductance dJ/dV at its operation point in the measurement condition has the most representation in the probed EQE. Because of the effects of the bias configurations on the operation conditions, a high bias-induced photocurrent(s) in the nontargeted subcell(s) and a medium bias voltage generally help to avoid measurement artifacts. If the J–V characteristic of the targeted subcell deforms with the illumination level and the operation current does not grow linearly with the photocurrent, the probed EQE will be dependent on the bias-light intensity for the targeted subcell beside the bias voltage. Thus the bias conditions for measurements should be configured according to the intended working condition of the multijunction cell.

Making use of the extra information from the model, the changes in the actually measured EQE in a quadruple-junction thin-film silicon-based solar cell with varied bias voltage were elucidated. It demonstrated how the modeling tool can assist the EQE measurements of multijunction cells. Not only it can make the acquired results less ambiguous, but combining with other optical or opto-electrical simulations it can also estimate the optimal bias configuration for an unfamiliar device even ahead of the actual experimental attempt. Such capability will be helpful in the research and development of two-terminal multijunction solar cells, especially the ones with novel or uncommon device structure.

Finally, attentions were raised to the interpretation of the measured spectral response. The EQE of the component subcells is meaningful information but generally it cannot be directly translated into the short-circuit current density of the multijunction cell. It was suggested that EQE measurements should be performed in a way that the measured EQE is related to a certain interested/relevant operation condition of the multijunction cell.

7. Experimental Section

In this paper, the origin of artifacts has been studied by modeling the EQE measurements of tandem (double-junction) solar cells. The simulations are based on a thin-film p-i-n a-Si:H/nc-Si:H tandem cell. The thickness of the absorber layers is 350 and 3000 nm, and the J_{ph} is 14.0 and 14.4 mA cm^{-2} for the top and bottom subcells, respectively. The genuine EQE spectra used for the simulations were adopted from the work by Tan et al.,[27] and are shown in Figure 2a (gray dashed lines). The quadruple-junction cell discussed in Section 3.4 is a thin-film p-i-n a-SiO$_x$:H/a-Si:H/nc-Si:H/nc-Si:H quadruple-junction solar cell. The thickness of the absorber layers is 67/380/1900/3200 nm and the device structure is the same as the one reported in the previous work.[18] The genuine EQE spectra required in the simulations were obtained by deliberate measurements on the studied cell and further confirmed with the result of optical simulations,[18] although it should be pointed out that the purpose of the simulations is to find out how the probed EQE may deviate from the genuine EQE. In this scenario, it is irrelevant whether or not the used EQE spectra accurately represent the original device.

The EQE measurements of the quadruple-junction cell were performed using an in-house system. The system uses a xenon light source and a 3-grating monochromator to provide a monochromatic light source, which was then chopped at a frequency of 123 Hz before reaching the devices. The current induced by this light was measured through a resistor with a lock-in amplifier. The measured value was

© 2016 The Authors. Published by WILEY-VCH Verlag GmbH & Co. KGaA, Weinheim

compared with the one from a calibrated reference diode to calculate the EQE. The bias light was provided by a selection from 8 different LEDs with adjustable intensity and with wavelengths of emission peak ranging from 350 to 940 nm. The voltage of the measured cell was biased via the control circuit. In addition, the temperature of the solar cell was controlled at 25 °C through the mounting stage. As for another input of the simulations, the spectral irradiance of the every light source was measured using a spectrometer (Avantes AvaSpec-2048 UA/IB) at the spot where the solar cell was mounted.

For every component subcell in the studied tandem and quadruple-junction solar cells, a single-junction cell was fabricated in order to acquire the parameters in the one-diode equation for the simulations. The single-junction cells have similar p-i-n structures to their counterparts in the multijunction cells, while their front and rear sides are covered by glass/transparent conductive oxide and Ag, respectively. The fabrication procedure and further details about the cell structures are reported elsewhere.[18,27] Illuminated *J–V* measurements were performed on the single-junction cells using a dual-lamp continuous solar simulator (WACOM WXS-90S-L2, class AAA) with an incident irradiance of 1000 W m^{-2}. Dark *J–V* measurements were performed using the same setup but shielding the cells from the light. During all measurements, the temperature of the cells was controlled at 25 °C. The one-diode equation was fitted with the measured *J–V* data to extract a set of diode parameters for every single-junction cell. The parameter sets were then used to simulate the *J–V* characteristics of the corresponding subcells.

Supporting Information

Supporting Information is available from the Wiley Online Library or from the author.

Acknowledgements

The authors thank René A. C. M. M. van Swaaij for the helpful discussions on the scientific content, Hairen Tan for providing the data of the studied tandem solar cell, Martijn van Sebille for the help on coding, Rudi Santbergen for giving advice on the manuscript, Remko Koornneef and Stefaan Heirman for the technical support.

This work was supported by the Foundation for Fundamental Research on Matter (FOM), which is part of the Netherlands Organization for Scientific Research (NWO).

Received: August 31, 2016
Revised: October 2, 2016
Published online:

[1] A. De Vos, *J. Phys. D Appl. Phys.* **1980**, *13*, 839.
[2] P. T. Chiu, D. Law, R. L. Woo, S. B. Singer, D. Bhusari, W. D. Hong, A. Zakaria, J. Boisvert, S. Mesropian, R. R. King, N. H. Karam, in *2014 IEEE 40th Photovolt. Spec. Conf.*, Denver, Colorado, USA, IEEE, **2014**, pp. 0011–0013.
[3] H. Sai, T. Matsui, T. Koida, K. Matsubara, M. Kondo, S. Sugiyama, H. Katayama, Y. Takeuchi, I. Yoshida, *Appl. Phys. Lett.* **2015**, *106*, 213902.
[4] M. A. Green, K. Emery, Y. Hishikawa, W. Warta, E. D. Dunlop, *Prog. Photovoltaics Res. Appl.* **2016**, *24*, 905.
[5] J. Burdick, T. Glatfelter, *Sol. Cells* **1986**, *18*, 301.
[6] M. Meusel, C. Baur, G. Létay, A. W. Bett, W. Warta, E. Fernandez, *Prog. Photovoltaics Res. Appl.* **2003**, *11*, 499.
[7] M. Pravettoni, R. Galleano, A. Virtuani, H. Müllejans, E. D. Dunlop, *Meas. Sci. Technol.* **2011**, *22*, 045902.
[8] J.-J. Li, S. H. Lim, C. R. Allen, D. Ding, Y.-H. Zhang, *IEEE J. Photovoltaics* **2011**, *1*, 225.
[9] V. Paraskeva, M. Hadjipanayi, M. Norton, M. Pravettoni, G. E. Georghiou, *Sol. Energy Mater. Sol. Cells* **2013**, *116*, 55.
[10] D. Bahro, M. Koppitz, A. Mertens, K. Glaser, J. Mescher, A. Colsmann, *Adv. Energy Mater.* **2015**, *5*, 1501019.
[11] C. J. Hibberd, F. Plyta, C. Monokroussos, M. Bliss, T. R. Betts, R. Gottschalg, *Sol. Energy Mater. Sol. Cells* **2011**, *95*, 123.
[12] T. Sogabe, A. Ogura, Y. Okada, *J. Appl. Phys.* **2014**, *115*, 074503.
[13] E. Barrigón, P. Espinet-González, Y. Contreras, I. Rey-Stolle, *Prog. Photovoltaics Res. Appl.* **2015**, *23*, 1597.
[14] R. Timmreck, T. Meyer, J. Gilot, H. Seifert, T. Mueller, A. Furlan, M. M. Wienk, D. Wynands, J. Hohl-Ebinger, W. Warta, R. A. J. Janssen, M. Riede, K. Leo, *Nat. Photonics* **2015**, *9*, 478.
[15] Standard *ASTM E2236-10*, **2015**.
[16] B. Yan, G. Yue, L. Sivec, J. Yang, S. Guha, C.-S. Jiang, *Appl. Phys. Lett.* **2011**, *99*, 113512.
[17] J.-W. Schuttauf, G. Bugnon, M. Stuckelberger, S. Hanni, M. Boccard, M. Despeisse, F.-J. Haug, F. Meillaud, C. Ballif, *IEEE J. Photovoltaics* **2014**, *4*, 757.
[18] F. T. Si, R. Santbergen, H. Tan, R. A. C. M. M. van Swaaij, A. H. M. Smets, O. Isabella, M. Zeman, *Appl. Phys. Lett.* **2014**, *105*, 063902.
[19] J.-W. Schüttauf, B. Niesen, L. Löfgren, M. Bonnet-Eymard, M. Stuckelberger, S. Hänni, M. Boccard, G. Bugnon, M. Despeisse, F.-J. Haug, F. Meillaud, C. Ballif, *Sol. Energy Mater. Sol. Cells* **2015**, *133*, 163.
[20] S. Kirner, S. Neubert, C. Schultz, O. Gabriel, B. Stannowski, B. Rech, R. Schlatmann, *Jpn. J. Appl. Phys.* **2015**, *54*, 08KB03.
[21] J. P. Mailoa, C. D. Bailie, E. C. Johlin, E. T. Hoke, A. J. Akey, W. H. Nguyen, M. D. McGehee, T. Buonassisi, *Appl. Phys. Lett.* **2015**, *106*, 121105.
[22] S. Albrecht, M. Saliba, J. P. Correa Baena, F. Lang, L. Kegelmann, M. Mews, L. Steier, A. Abate, J. Rappich, L. Korte, R. Schlatmann, M. K. Nazeeruddin, A. Hagfeldt, M. Grätzel, B. Rech, *Energy Environ. Sci.* **2016**, *9*, 81.
[23] J. Werner, C.-H. Weng, A. Walter, L. Fesquet, J. P. Seif, S. De Wolf, B. Niesen, C. Ballif, *J. Phys. Chem. Lett.* **2016**, *7*, 161.
[24] T. Todorov, T. Gershon, O. Gunawan, Y. S. Lee, C. Sturdevant, L.-Y. Chang, S. Guha, *Adv. Energy Mater.* **2015**, *5*, 1500799.
[25] C. D. Bailie, M. G. Christoforo, J. P. Mailoa, A. R. Bowring, E. L. Unger, W. H. Nguyen, J. Burschka, N. Pellet, J. Z. Lee, M. Grätzel, R. Noufi, T. Buonassisi, A. Salleo, M. D. McGehee, *Energy Environ. Sci.* **2015**, *8*, 956.
[26] H. Tan, A. Furlan, W. Li, K. Arapov, R. Santbergen, M. M. Wienk, M. Zeman, A. H. M. Smets, R. A. J. Janssen, *Adv. Mater.* **2016**, *28*, 2170.
[27] H. Tan, E. Moulin, F. T. Si, J.-W. Schüttauf, M. Stuckelberger, O. Isabella, F.-J. Haug, C. Ballif, M. Zeman, A. H. M. Smets, *Prog. Photovoltaics Res. Appl.* **2015**, *23*, 949.
[28] D. Bahro, M. Koppitz, A. Colsmann, *Nat. Photonics* **2016**, *10*, 354.
[29] R. Timmreck, T. Meyer, J. Gilot, H. Seifert, T. Mueller, A. Furlan, M. M. Wienk, D. Wynands, J. Hohl-Ebinger, W. Warta, R. A. J. Janssen, M. Riede, K. Leo, *Nat. Photonics* **2016**, *10*, 355.
[30] J. Merten, J. M. Asensi, C. Voz, A. V. Shah, R. Platz, J. Andreu, *IEEE Trans. Electron Devices* **1998**, *45*, 423.
[31] S. S. Hegedus, W. N. Shafarman, *Prog. Photovoltaics Res. Appl.* **2004**, *12*, 155.
[32] R. Timmreck, K. Leo, M. Riede, *Prog. Photovoltaics Res. Appl.* **2015**, *23*, 1353.
[33] K. Söderström, G. Bugnon, R. Biron, C. Pahud, F. Meillaud, F.-J. Haug, C. Ballif, *J. Appl. Phys.* **2012**, *112*, 114503.
[34] J. Gilot, M. M. Wienk, R. A. J. Janssen, *Adv. Funct. Mater.* **2010**, *20*, 3904.
[35] L. J. A. Koster, M. Kemerink, M. M. Wienk, K. Maturová, R. A. J. Janssen, *Adv. Mater.* **2011**, *23*, 1670.
[36] W. Tress, K. Leo, M. Riede, *Phys. Status Solidi - Rapid Res. Lett.* **2013**, *7*, 401.
[37] S. H. Lim, J.-J. Li, E. H. Steenbergen, Y.-H. Zhang, *Prog. Photovoltaics Res. Appl.* **2013**, *21*, 344.

© 2016 The Authors. Published by WILEY-VCH Verlag GmbH & Co. KGaA, Weinheim